Pergamon

Int. J. Heat Mass Transfer. Vol. 40, No. 14, pp. 3283–3291, 1997

Printed in Great Britain
0017–9310/97 $17.00+0.00

PII: S0017–9300(96)00388–2

Convective heat transfer due to thermocapillary convection with a strong magnetic field parallel to the free surface

T. E. MORTHLAND and J. S. WALKER†

Department of Mechanical and Industrial Engineering, University of Illinois, Urbana–Champaign, 1206 West Green Street, Urbana, IL 61801, U.S.A.

(*Received* 8 *May* 1996 *and in final form* 12 *November* 1996)

Abstract—This paper treats the motion and heat transfer in an electrically conducting fluid that is bounded by two parallel, isothermal walls, and by a plane free surface. Gradients in the surface tension of the free surface drive a strong recirculating thermocapillary convection. In the presence of a magnetic field which is parallel to the free surface, the thermocapillary convection is confined to a thin boundary layer adjacent to the free surface. Only when the Péclet number is at least $O(Ha^{1/4})$, where Ha is the large Hartmann number, is the heat flux entering the free surface redistributed by thermal convection inside the boundary layer before entering the quiescent core. This problem is a model of the floating-zone growth of semiconductor crystals with a uniform, axial magnetic field. © 1997 Elsevier Science Ltd.

1. INTRODUCTION

In the floating-zone process, a single crystal is grown from a cylindrical melt which is held by surface tension between the growing single crystal and the melting feed rod. A heat source keeps the liquid temperature above the solidification temperature, and causes large temperature gradients along the free surface. Since the surface tension increases from the hottest part at the center of the free surface to the cold parts at the crystal and feed rod, the surface-tension gradients drive two thermocapillary circulations in opposite directions above and below the center of the free surface.

The thermocapillary convection is unsteady when the temperature difference along the free surface is more than 1 K for a typical semiconductor process [1]. The unsteady thermocapillary convection is undesirable since it produces periodic spatial variations of the dopant concentrations in the crystal (striations), which in turn lead to faulty electronic devices. Since molten semiconductors are good electrical conductors, an externally applied, steady magnetic field can eliminate the unsteady motion, and reduce the strength of the residual steady motion in the melt [2]. There are no striations in a large part of a crystal grown by the floating-zone process with a strong axial magnetic field [1, 3]. Numerical simulations have shown that a magnetic field can eliminate unsteady thermocapillary convection [4, 5]. For the floating-zone process, an axial magnetic field is parallel to the essentially cylindrical free surface. This contrasts with the Czochralski process where an axial magnetic field is perpendicular to the horizontal free surface.

For typical axial magnetic field strengths ($B = 0.1$–1.0 T), the thermocapillary convection is confined to a thin parallel layer which lies between the free surface and a quiescent core region. For the heat transfer from the free surface to the colder crystal and feed rod, there is only conduction in the core, while convection may be comparable to conduction in the parallel layer if the Péclet number, Pe, is sufficiently large.

A previous paper [6] presented numerical solutions for the flow patterns in various floating-zone geometries, but this previous work did not include the effects of convective heat transfer or inertia. Here is presented an asymptotic solution for a strong magnetic field. While numerical solutions are still needed for the flow and heat transfer in the parallel layer, the computational requirements are far less than those for a fully numerical solution for some magnetic field strengths. In addition, the asymptotic analysis reveals parametric trends more readily than fully numerical treatments, and serves as a complement to the latter.

Using an asymptotic analysis, Hjellming and Walker [7] showed that the heat flux is redistributed by a parallel layer with an O(1) flow through it when $Pe = O(1)$. Since the present thermocapillary convection is confined to the parallel layer, there are equal and opposite O(1) flows inside this layer, so that the convective heat transfers cancel, and there is no redistribution of the heat flux for $Pe = O(1)$. With the flow entirely confined to the parallel layer, Pe must be

†Author to whom correspondence should be addressed.

NOMENCLATURE

A_n	separation-of-variable coefficient
B	characteristic magnetic flux density
d	width of truncated domain
F	integration function
G_{kl}	variable coefficient
Ha	Hartmann number, $BL(\sigma/\mu)^{1/2}$
j_z	electric current density in z-direction
L	characteristic length
N	interaction parameter, $\sigma B^2 L/\rho U$
P	nondimensional pressure
Pe	Péclet number, UL/κ
Pr	Prandtl number, $\mu/\rho\kappa$
q	maximum nondimensional heat flux
R_m	magnetic Reynolds number, $\mu_p\sigma UL$
T	nondimensional temperature
T^*	dimensional temperature
T_s^*	temperature at walls
ΔT^*	characteristic temperature difference
U	characteristic velocity
u	nondimensional x-velocity
v	nondimensional y-velocity
x, y, z	Cartesian coordinates.

Greek symbols

α	$N^{-1}\,Ha^{3/2}$
γ	$Pe\,Ha^{-1/4}$
δ	$Ha^{1/4}$
Γ	surface tension
κ	thermal diffusivity
λ_k	$(k\pi/2)^{1/2}$, k = integer
μ	absolute viscosity
μ_p	magnetic permeability
ξ	stretched coordinate, $Ha^{1/2}\,x$
ρ	density
σ	electrical conductivity
ψ	nondimensional stream function
ψ^*	dimensional stream function, $UL\psi$.

Subscripts

c	core region
h	Hartmann layer
I	intersection region
p	parallel region.

large, namely $O(Ha^{1/4})$, where Ha is the large Hartmann number, before convective heat transfer redistributes the heat flux.

2. PROBLEM FORMULATION

The plane, dimensionless geometry is presented in Fig. 1. An incompressible, electrically conducting liquid is bounded by two parallel, isothermal walls at dimensional temperature T_s^*, and by a plane free surface which is perpendicular to the walls. With half the distance between the parallel walls as the characteristic length L, and with the origin at the center of the free surface, the liquid occupies the region $-\infty < x \leqslant 0$, $-1 \leqslant y \leqslant 1$. There is an applied, uniform, steady magnetic field which is perpendicular to the walls.

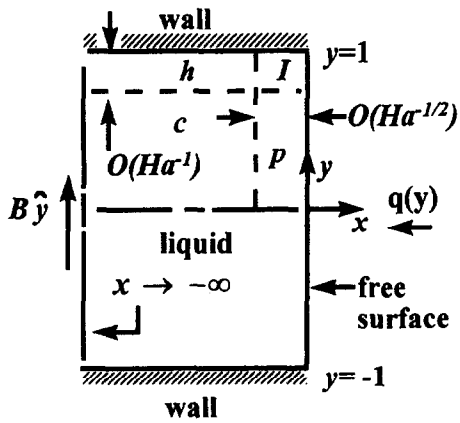

Fig. 1. Model problem showing asymptotic subregions for $Ha \gg 1$.

The electric current in the liquid produces an 'induced' magnetic field, which is superimposed on the externally applied field. The magnetic Reynolds number, $R_m = \mu_p\sigma UL$, is the characteristic ratio of the induced to the applied magnetic field strength. Here μ_p and σ are the magnetic permeability and electrical conductivity of the liquid, while the appropriate characteristic velocity for magnetically suppressed thermocapillary convection [8] is

$$U = \frac{(-d\Gamma/dT^*)\Delta T^*}{BL(\sigma\mu)^{1/2}}. \tag{1}$$

Here the surface tension Γ is assumed to decrease linearly with increasing dimensional temperature T^*, so that $d\Gamma/dT^*$ is a negative constant, while ΔT^* is the maximum elevation of the free-surface temperature above T_s^*, B is the characteristic magnetic flux density of the applied field, and μ is the liquid's viscosity. For a typical gallium arsenide GaAs floating-zone process with $\Delta T^* = 15$ K and $B = 0.5$ T [1], $U = 5$ mm s^{-1}, and $R_m = 0.0001$. Therefore, the induced magnetic field is neglected, so that the magnetic field, normalized by B, is simply a unit vector in the y-direction. For GaAs, $\sigma = 0.65$ MS m^{-1}, $\rho = 5710$ kg m^{-3}, $\mu = 0.00278$ Pa s, and $d\Gamma/dT^* = -0.18$ mN m^{-1} K^{-1}, and $L = 2.54$ cm is used.

Table 1. Values of parameters for various magnetic-flux densities

B (T)	U [mm s^{-1}]	N	Ha	Pe	α	γ
0.1	25.03	1.2	38.9	88.3	209.801	35.361
0.2	12.51	9.2	77.7	44.1	74.176	14.867
0.3	8.34	31.2	116.6	29.4	40.376	8.956
0.4	6.26	73.9	155.5	22.1	26.225	6.251
0.5	5.00	144.4	194.4	17.7	18.765	4.729
0.6	4.17	249.5	233.2	14.7	14.275	3.766
0.75	3.34	487.4	291.6	11.8	10.214	2.849
1.0	2.50	1155.2	388.7	8.8	6.634	1.988
10.0	0.25	1.2E+6	3887.4	0.9	0.210	0.112

For a steady, two-dimensional flow:

$$N^{-1}\left(u\frac{\partial u}{\partial x}+v\frac{\partial u}{\partial y}\right)=-\frac{\partial P}{\partial x}-j_z+Ha^{-2}\left(\frac{\partial^2 u}{\partial x^2}+\frac{\partial^2 u}{\partial y^2}\right) \tag{2a}$$

$$N^{-1}\left(u\frac{\partial v}{\partial x}+v\frac{\partial v}{\partial y}\right)=-\frac{\partial P}{\partial y}+Ha^{-2}\left(\frac{\partial^2 v}{\partial x^2}+\frac{\partial^2 v}{\partial y^2}\right) \tag{2b}$$

$$j_z=u\quad \frac{\partial u}{\partial x}+\frac{\partial v}{\partial y}=0$$

$$Pe\left(u\frac{\partial T}{\partial x}+v\frac{\partial T}{\partial y}\right)=\frac{\partial^2 T}{\partial x^2}+\frac{\partial^2 T}{\partial y^2}. \tag{2c–e}$$

Here u and v are the x- and y-components of the velocity normalized by U, P is the pressure normalized by σUB^2L, j_z is the z-component of the electric current density normalized by σUB, and $T=(T^*-T_s^*)/\Delta T^*$. The interaction parameter N, Ha and Pe are defined by

$$N=\frac{\sigma B^2 L}{\rho U}\quad Ha=BL\left(\frac{\sigma}{\mu}\right)^{1/2}\quad Pe=UL/\kappa$$

where ρ and κ are the density and thermal diffusivity of the liquid. Equations (2a) and (2b) are the x- and y-components of the Navier–Stokes equation with the electromagnetic (EM) body force due to j_z, equation (2c) is the z-component of Ohm's law with no electric field because there is no electric field in an axisymmetric floating zone, equation (2d) is the continuity equation, and equation (2e) is the heat equation neglecting Joulean heating and viscous dissipation [9]. The values of U, N, Ha and Pe for a typical GaAs floating zone, and for values of B between 0.1 and 10 T, are given in Table 1. It is noted that Pe decreases as the magnetic field strength is increased since U varies inversely with B.

The floating zone is melted by a heat flux at the free surface given by

$$\frac{\partial T}{\partial x}=q(1-y^2)\quad \text{at}\quad x=0. \tag{3a}$$

This quadratic heat flux has been used by Müller and Rupp [4] to model optically-heated floating zones. The free surface heat flux is symmetric about $y=0$, so that the flow and temperature are also symmetric about $y=0$, and only the domain given by $-\infty<x\leqslant 0$ and $0\leqslant y\leqslant 1$ is modeled. The other boundary conditions at the wall and free surface are

$$u=v=T=0\quad \text{at}\quad y=1 \tag{3b}$$

$$u=0\quad \frac{\partial v}{\partial x}=-Ha\frac{\partial T}{\partial y}\quad \text{at}\quad x=0. \tag{3c,d}$$

Equation (3d) reflects a balance between the viscous shear stress and the gradient of the surface tension. The symmetry conditions are

$$v=\frac{\partial u}{\partial y}=\frac{\partial T}{\partial y}=0\quad \text{at}\quad y=0. \tag{3e}$$

Since ΔT^* is defined as the maximum free-surface temperature difference:

$$T=1\quad \text{at}\quad x=y=0 \tag{3f}$$

which determines q. Whatever heat flux is needed to maintain a given free-surface temperature difference is provided.

It is assumed that B is sufficiently large that $Ha\gg 1$ and $N\gg 1$, so that simplified versions of equations (2) can be solved in various subregions of the domain. The subregions (shown in Fig. 1) are the inviscid, inertialess core (c), the Hartmann layer (h), with an $O(Ha^{-1})$ thickness adjacent to the wall at $y=1$, the parallel layer (p), with an $O(Ha^{-1/2})$ thickness adjacent to the free surface at $x=0$, and the intersection region (I) with $O(Ha^{-1/2})\times O(Ha^{-1})$ dimensions.

The coupled asymptotic analyses for the core and Hartmann layer show that u, v, j_z and P are zero in both subregions to all orders of Ha and N. The thermocapillary convection inside the parallel layer does not perturb the stagnant fluid in the core. The temperature in the core and Hartmann-layer subregions is given by $T_c=\Sigma_{k=0}^{\infty}\delta^k T_{ck}(x,y)$, where the small parameter δ will be determined by matching the parallel-layer temperature T_p. Equation (2e) gives

$$\frac{\partial^2 T_{ck}}{\partial x^2}+\frac{\partial^2 T_{ck}}{\partial y^2}=0 \tag{4}$$

for all k. Equations (3b) and (3e) apply to each T_{ck}.

The separation-of-variables solution for $k = 0$ (or any k) is

$$T_{c0} = \sum_{n=0}^{\infty} A_n \exp[(n+1/2)\pi x] \cos[(n+1/2)\pi y] \quad (5)$$

where the coefficients A_n will be determined by matching T_p. The heat flux entering the liquid at the free surface may be redistributed by the convection inside the parallel layer, so that equation (3a) may not apply to T_c.

For the parallel layer, the stretched coordinate $\xi = Ha^{1/2} x$ is introduced. The choice for ΔT^* means that T_p is O(1), equation (3d) indicates that v_p is $O(Ha^{1/2})$, equation (2d) indicates that u_p is O(1), equation (2c) indicates that j_{zp} is O(1), and equation (2a) indicates that P_p is $O(Ha^{-1/2})$. The appropriate asymptotic expansions are

$$v_p = Ha^{1/2} \sum_{k=0}^{\infty} \delta^k v_{pk}(\xi, y) \quad u_p = j_{zp} = \sum_{k=0}^{\infty} \delta^k u_{pk}(\xi, y) \quad (6a, b)$$

$$P_p = Ha^{-1/2} \sum_{k=0}^{\infty} \delta^k P_{pk}(\xi, y) \quad T_p = \sum_{k=0}^{\infty} \delta^k T_{pk}(\xi, y). \quad (6c, d)$$

The parallel-layer solution depends on the relationship between the two large parameters Ha and N. It is assumed that $N = \alpha^{-1} Ha^{3/2}$, where α is an O(1) parameter, so that inertial and viscous effects are comparable for the thermocapillary convection inside the parallel layer. If $\alpha = 0$, the solution becomes the inertialess solution [6]. In theory, as $\alpha \to \infty$, the parallel layer splits into a thicker inviscid inertial layer with an $O(N^{-1/3})$ thickness and a thinner viscous layer with an $O(Ha^{-1/2})$ thickness [10]. However, it appears that, as α increases past some unknown critical value, an instability occurs, and the steady, two-dimensional flow changes to an unsteady three-dimensional flow [4], so that no steady, two-dimensional flow actually exists for $N \gg Ha^{3/2}$. A treatment of this stability problem will be presented in a future paper.

The leading terms in equation (2a)–(2d) give

$$0 = -\frac{\partial P_{p0}}{\partial \xi} - u_{p0} \quad (7a)$$

$$\alpha\left[u_{p0}\frac{\partial v_{p0}}{\partial \xi} + v_{p0}\frac{\partial v_{p0}}{\partial y}\right] = -\frac{\partial P_{p0}}{\partial y} + \frac{\partial^2 v_{p0}}{\partial \xi^2} \quad (7b)$$

$$\frac{\partial u_{p0}}{\partial \xi} + \frac{\partial v_{p0}}{\partial y} = 0. \quad (7c)$$

Equation (7c) leads to a stream function $\psi_0(\xi, y)$, where

$$u_{p0} = \frac{\partial \psi_0}{\partial y} \quad v_{p0} = -\frac{\partial \psi_0}{\partial \xi}. \quad (8a, b)$$

Equation (1) for U leads to an O(1) stream function inside the parallel layer, i.e. the magnitude of the dimensionless circulation approaches a constant value as B becomes large, so that the dimensional circulation decreases as B^{-1}. Since the O(1) circulation is confined to a thin layer, v is large. Equations (7a) and (8a) lead to another integration function $F_0(\xi, y)$, where

$$\psi_0 = \frac{\partial F_0}{\partial \xi} \quad P_{p0} = -\frac{\partial F_0}{\partial y} \quad (9a, b)$$

$$u_{p0} = \frac{\partial^2 F_0}{\partial \xi\, \partial y} \quad v_{p0} = -\frac{\partial^2 F_0}{\partial \xi^2} \quad (9c, d)$$

Equation (7b) gives the equation governing F_0:

$$\alpha\left[\frac{\partial^2 F_0}{\partial \xi^2}\frac{\partial^3 F_0}{\partial \xi^2\, \partial y} - \frac{\partial^2 F_0}{\partial \xi\, \partial y}\frac{\partial^3 F_0}{\partial \xi^3}\right] = \frac{\partial^2 F_0}{\partial y^2} - \frac{\partial^4 F_0}{\partial \xi^4}. \quad (10)$$

Here ψ_0 and F_0 are the leading terms in asymptotic expansions which are the same as equation (6b) and (6c), respectively, for the O(1) stream function ψ and the $O(Ha^{-1/2})$ integration function F. There are arbitrary additive constants in ψ and F which are eliminated by setting $\psi = F = 0$ at $\xi = 0$ and $y = 0$. The intersection region (I) matches any value of u_p at $y = 1$, as long as

$$v_p = 0 \quad \text{at} \quad y = 1 \quad (11)$$

neglecting $O(Ha^{-1/2})$ terms [11]. Equations (3c)–(3f) and (11), and matching the stagnant core, give the boundary conditions on F_0:

$$\frac{\partial F_0}{\partial \xi} = 0 \quad \frac{\partial^3 F_0}{\partial \xi^3} = \frac{\partial T_{p0}}{\partial y} \quad \text{at} \quad \xi = 0 \quad (12a, b)$$

$$F_0 = 0 \quad \frac{\partial^2 F_0}{\partial y^2} = 0 \quad \text{at} \quad y = 0 \quad (12c, d)$$

$$F_0 = 0 \quad \text{at} \quad y = 1 \quad (12e)$$

$$F_0 \to 0 \quad \text{as} \quad \xi \to -\infty. \quad (12f)$$

For sufficiently small values of Pe, the flow has no effect on the O(1) temperature, i.e. the A_n in equation (5) are determined by applying equation (3a) to $\partial T_{c0}/\partial x$ at $x = 0$, and the $\partial T_{p0}/\partial y$ at $\xi = 0$ in equation (12b) is simply $\partial T_{c0}/\partial y$ at $x = 0$. In this limit, the thermocapillary convection is driven by a fixed free-surface temperature gradient, and only depends on α [12]. The present paper is focused on values of Pe which are large enough that the thermocapillary convection inside the parallel layer changes the free-surface temperature from that for pure thermal conduction, so that the temperature and flow problems are coupled. This coupling occurs when Pe is comparable to $Ha^{1/4}$, so that $Pe = \gamma\, Ha^{1/4}$ is introduced, where γ is an O(1) parameter. The δ in the expansion for T_c and in equations (6) is $Ha^{-1/4}$. Equation (3a) gives the boundary conditions

$$\frac{\partial T_{p0}}{\partial \xi} = \frac{\partial T_{p1}}{\partial \xi} = 0 \quad \frac{\partial T_{p2}}{\partial \xi} = q_0(1-y^2) \quad \text{at} \quad \xi = 0 \quad (13a, b)$$

where $q = \Sigma_{k=0}^{\infty} Ha^{-k/4} q_k$. Matching the core temperature gives the conditions

$$T_{p0} \to T_{c0}(0, y) \quad T_{p1} \to T_{c1}(0, y) \qquad (14a, b)$$

$$T_{p2} \to \xi \frac{\partial T_{c0}}{\partial x}(0, y) + T_{c2}(0, y) \qquad (14c)$$

as $\xi \to -\infty$. Equation (2e) gives

$$\frac{\partial^2 T_{p0}}{\partial \xi^2} = 0 \qquad (15)$$

and the solution which satisfies equations (13a) and (14a) is $T_{p0}(\xi, y) \equiv T_{c0}(0, y)$. Equation (2e) now gives

$$\frac{\partial^2 T_{p1}}{\partial \xi^2} = -\gamma \frac{\partial T_{c0}}{\partial y}(0, y) \frac{\partial^2 F_0}{\partial \xi^2}(\xi, y). \qquad (16)$$

The solution which satisfies equations (12a), (12f), (13b) and (14b) is

$$T_{p1}(\xi, y) = T_{c1}(0, y) - \gamma \frac{\partial T_{c0}}{\partial y}(0, y) F_0(\xi, y). \qquad (17)$$

Now equation (2e) gives

$$\frac{\partial^2 T_{p2}}{\partial \xi^2} = \gamma \left[\frac{\partial^2 F_0}{\partial \xi \partial y} \frac{\partial T_{p1}}{\partial \xi} - \frac{\partial^2 F_0}{\partial \xi^2} \frac{\partial T_{p1}}{\partial y} - \frac{\partial T_{c0}}{\partial y}(0, y) \frac{\partial^2 F_1}{\partial \xi^2} \right]. \qquad (18)$$

Equations (13b) and (14c) give

$$\frac{\partial T_{c0}}{\partial x}(0, y) = q_0(1 - y^2) - \int_{-\infty}^{0} \frac{\partial^2 T_{p2}}{\partial \xi^2}(\xi, y)\, d\xi. \qquad (19)$$

When equations (17) and (18) are introduced into equation (19), the integrals of the terms involving F_1 and $T_{c1}(0, y)$ are both zero because F_1 also satisfies equations (12a) and (12f). After integrations by parts with the same equations, equation (19) becomes

$$\frac{\partial T_{c0}}{\partial x}(0, y) = q_0(1 - y^2) + \gamma^2 \frac{d}{dy} \times \left(\frac{\partial T_{c0}}{\partial y}(0, y) \int_{-\infty}^{0} \left[\frac{\partial F_0}{\partial \xi}(\xi, y) \right]^2 d\xi \right). \qquad (20)$$

The last term represents the redistribution of the heat flux in the y-direction due to the thermocapillary convection inside the parallel layer. The integral in the last term is

$$\int_{-\infty}^{0} \psi_0^2\, d\xi,$$

so that it increases from zero at $y = 0$ to a maximum where the circulation is maximum, and then decreases to zero at $y = 1$. Since the integral of the last term from $y = 0$ to $y = 1$ is zero, the total heat flux into the core equals the total heat flux into the free surface, i.e. there is no O(1) heat flux from the parallel layer to the wall, as one would expect, since the parallel-layer equation does not include conduction in the y-direction. Equation (20) indicates that the heat flux into the free surface is transferred in the y-direction from below the level of maximum circulation to above this level before it enters the core.

Equation (12b) is replaced by

$$\frac{\partial^3 F_0}{\partial \xi^3} = \frac{\partial T_{c0}}{\partial y}(0, y) \quad \text{at} \quad \xi = 0. \qquad (21)$$

Equations (10), (12a), (12c)–(12f) and (21) govern $F_0(\xi, y)$, while the A_n in equation (5) are determined by equation (20), which is a non-linear equation because F_0 depends on $\partial T_{c0}/\partial y$ at $x = 0$. We solve for F_0 with a Chebyshev spectral collocation method. To the column of unknown coefficients in the double Chebyshev polynomial expansion for F_0 on the domain truncated at $\xi = -12$ are added the coefficients A_n in equation (5), so that we solved for F_0 and T_{c0} simultaneously. Since equations (10) and (20) are non-linear, the solution is iterated, using the previous solution for the second-order derivatives on the left-hand side of equation (10), and for $\partial F_0/\partial \xi$ in equation (20). The truncated integral in equation (20) was evaluated with a trapezoidal quadrature with at least eight points between any adjacent zeros of the most oscillatory Chebyshev polynomial.

3. INERTIALESS SOLUTION FOR $N \gg Ha^{3/2}$

For $\alpha \ll 1$, the separation-of-variables solution for equations (10), (12a), (12c)–(12f) and (21), with equation (5), is

$$F_0 = \sum_{k=1}^{\infty} B_k \sin(k\pi y) \exp(\lambda_k \xi)[\sin(\lambda_k \xi) - \cos(\lambda_k \xi)] \qquad (22a)$$

$$B_k = \frac{2\lambda_k(-1)^k}{k\pi^2} \sum_{n=0}^{\infty} A_n \frac{(-1)^n(n + 1/2)}{[k^2 - (n + 1/2)^2]} \qquad (22b)$$

where $\lambda_k = (k\pi/2)^{1/2}$. The integral in equation (20) can be evaluated analytically:

$$\int_{-\infty}^{0} \left(\frac{\partial F_0}{\partial \xi} \right)^2 d\xi = 2 \sum_{k=1}^{\infty} \sum_{l=1}^{\infty} G_{kl} \sin(k\pi y) \sin(l\pi y) \qquad (23a)$$

$$G_{kl} = \frac{\pi B_k B_l k l}{2(k + l)(\lambda_k + \lambda_l)}. \qquad (23b)$$

Equations (5) and (23a) are introduced into equation (20), which is then multiplied by $\cos[(m + 1/2)\pi y]$ and integrated from $y = 0$ to $y = 1$ in order to obtain a set of algebraic equations for the coefficients A_n in equation (5), and for the heat flux q_0:

$$A_m + 4\pi\gamma^2 \sum_{n=0}^{\infty} A_n(n+1/2) \sum_{k=1}^{\infty}\sum_{l=1}^{\infty} G_{kl}F_{mnkl}$$

$$-\frac{4(-1)^m}{\pi^4(m+1/2)^4} q_0 = 0 \quad \text{for } m = 0, 1, 2, 3, \ldots \tag{24a}$$

$$F_{mnkl} = \tfrac{1}{8}[Q(m-n+k-l) + Q(m-n-k+l) + Q(m+n+1-k-l) - Q(m-n+k+l) - Q(m-n-k-l) - Q(m+n+1+k-l) - Q(m+n+1-k+l)] \tag{24b}$$

where $Q(0) = 1$, and $Q(i) = 0$ for $i \neq 0$. Equation (3f) gives the only inhomogeneous equation:

$$\sum_{n=0}^{\infty} A_n = 1. \tag{25}$$

Equations (22b) and (23b) show that G_{kl} depend on A_n, so that equations (24a) and (25) for A_n and q_0 are nonlinear. In the iterative solution, the last set of values of A_n was used to determine G_{kl} through equations (22b) and (23b), and then the truncated equations (24a) and (25) were solved for the next set of values of A_n and q_0 using Gauss elimination. For the smallest nonzero value of γ, the A_n for $\gamma = 0$ was used for the first values of G_{kl}. For each successively larger value of γ, the converged values of A_n for the previous value of γ were used for the first values of G_{kl}.

The values for α and γ in Table 1 show that α is larger than γ for our typical GaAs floating zone. In the next section are presented the spectral collocation solutions for the pairs of values of α and γ in Table 1 for $B = 10.0$, 1.0, 0.75 and 0.6 T, where the $B = 10.0$ T case is a base case for $\alpha \ll 1$ and $\gamma \ll 1$. Also presented are the spectral solutions for the same values of α with $\gamma = 0$, and for the same values of γ with $\alpha = 0$, in order to separate the effects of inertia and convective heat transfer. The analytical solution for $\alpha = 0$ presented in this section served as a benchmark to test the accuracy of the numerical spectral collocation solution. The numerical results for $\alpha = 0$ and for all cases of γ agreed extremely well with the analytical results.

Since $\gamma = Pr\, Ha^{1/4}\alpha$, where $Pr = \mu/\rho k$ is the Prandtl number, liquid-metal thermocapillary convection in much larger geometries with much stronger magnetic fields might have significant values of γ for small values of α, in spite of the small values of Pr. For such cases, the present analytical solution would be much better than a numerical solution since it requires a very small fraction of the computational resources for the same accuracy.

4. RESULTS AND DISCUSSION

Magnetic field strengths of 10.0, 1.0, 0.75 and 0.6 T were chosen for the results presented in Section 4.1. These magnetic field strengths correspond to values of $\alpha = 0.210$, 6.634, 10.214 and 14.275, and $\gamma = 0.112$, 1.988, 2.849 and 3.766, respectively, as shown in Table 1. The results for the same values of α and $\gamma = 0$ are presented in Section 4.2 in order to study inertial effects without convective heat transfer, i.e. with a fixed free-surface temperature. The results for the same values of γ and $\alpha = 0$ are presented in Section 4.3 in order to study the effects of convective heat transfer without inertial effects. The results in Section 4.3 were computed with the spectral code for arbitrary values of α and γ, and with the analytical solution in Section 3 for $\alpha = 0$. The excellent agreement between the two sets of results for every value of γ provided a validation of the spectral code's accuracy. For the spectral code, the semi-infinite domain was truncated at $\xi = -d$, and symmetry conditions were applied here. The value of d was increased until the results were independent of d. Only the odd Chebyshev polynomials in $(\xi + d)/d$ and y were included because of symmetries. Variation of the numbers of polynomials showed that 30 polynomials in each direction were sufficient to give excellent results for every case. Equation (5) for T_{c0} was truncated at $n = 30$ for all cases, except those for $B = 0.6$ T. For $B = 0.6$ T, convective heat transfer produces a very large heat flux to the core near $y = 1$, and 40 terms in equation (5) were needed in order to capture this extreme heat flux accurately.

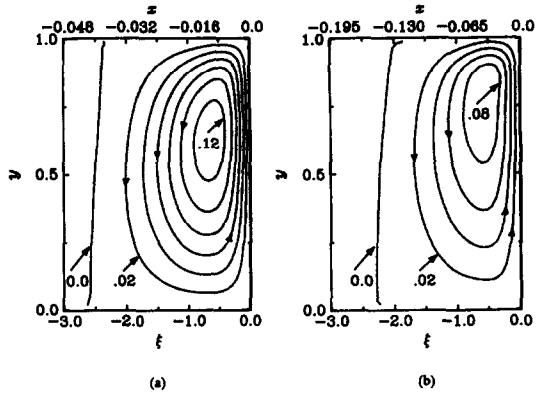

(a) (b)

Fig. 2. Contours of the nondimensional stream function ψ for: (a) $B = 10.0$ T with $\psi = 0.02k$, for $k = 0$–6 and (b) $B = 0.6$ T with $\psi = 0.02k$, for $k = 0$–4.

4.1. *Variable magnetic flux density* B

The streamlines for $B = 10.0$ T and $B = 0.6$ T are shown in Fig. 2(a) and (b), respectively. The top and bottom horizontal axes are the unstretched x and stretched ξ coordinates, respectively. For $-1 \leqslant y \leqslant 0$, there is a clockwise circulation given by the mirror image of the streamlines in Fig. 2. The widths of the parallel layers are $\Delta x = 0.04$ or $2.5Ha^{-1/2}$ for $B = 10$ T, and $\Delta x = 0.15$ or $2.3Ha^{-1/2}$ for $B = 0.6$ T. The width Δx of the recirculation grows as B decreases since fluid traveling across the magnetic field experiences a weaker EM body force. The location and magnitude of the maximum value of the stream function ψ_{max} also change with B, and these changes affect the convective heat transfer in the recirculating flow. At 10.0 T, $\psi_{max} = 0.136$ at $x = -0.010$

and $y = 0.640$, while, at 0.6 T, $\psi_{max} = 0.097$ at $x = -0.037$ and $y = 0.770$. For $\alpha = 0.210$, inertial effects are negligible, so that only the viscous force and the EM body force oppose the acceleration of the flow by the surface-tension gradient. For $\alpha = 14.275$, the surface-tension gradient must also overcome a large inertial 'force' opposing the acceleration, so that ψ_{max} is smaller. The delay in the acceleration of fluid particles due to inertial opposition shifts the location of ψ_{max} in the flow direction, i.e. toward the wall.

The maximum dimensional circulation $\psi^* = UL\psi$ decreases as B is increased. For example, at 10.0, 1.0, 0.75 and 0.6 T, $10^5\psi^*_{max} = 0.10, 0.72, 0.87$ and $1.04\ m^2\ s^{-1}$, respectively, i.e. about a 10-fold increase in the volumetric flow rate per unit length.

The free-surface temperature distributions $T_{c0}(0, y)$ for $B = 10.0$ T and $B = 0.6$ T are shown in Fig. 3(a). As B changes from 10.0 T to 0.6 T, $T_{c0}(0, y)$ decreases for $0 < y \leqslant 0.75$, and increases for $0.75 \leqslant y < 1$. Since $Pe = 14.7$ and 0.9 at $B = 0.6$ and 10.0 T, the convection of internal energy is greater at $B = 0.6$ T. As noted in Section 2, the convective heat transfer in the parallel layer transfers the heat flux entering the free surface from the plane of symmetry toward the wall.

Before entering the core region, the heat flux entering the free surface is redistributed by convection inside the recirculating flow in the parallel layer. The amount of the heat flux that is redistributed inside the parallel layer depends on the magnitude of Pe, which in turn is a function of B (see Table 1). The asymptotic analysis showed that the heat flux into the core is first affected when $Pe = O(Ha^{1/4})$, so it would be expected to see a change only when $\gamma \geqslant 1$. The variation of the core heat flux $\partial T_{c0}/\partial x(0, y)$ is shown in Fig. 3(b) for $B = 10.0$, 1.0, 0.75 and 0.6 T. For $B = 10.0$ T $\gamma = 0.210$, so the effects of convective heat transfer are negligible, and the core heat flux is equal to the parabolic heat flux entering the free surface, even though $Pe = O(1)$, namely $Pe = 0.9$. With an O(1) Pe, the flow adjacent to the free surface, moving from the center of the free surface towards the wall at $y = 1$, convects heat upward. However, the flow further from the free surface, moving from the wall towards the plane of symmetry, convects heat downward, exactly canceling the effect of the upward flow. At $B = 1.0$, 0.75 and 0.6 T, the value of $Pe = 8.8$, 11.8 and 14.7, while the value of $\gamma = 1.988$, 2.849 and 3.766, respectively. Figure 3(b) shows the redistribution of the heat flux for these values of B, and indicates that, as the magnetic field strength is reduced, convective heat transfer grows stronger. This effect is evident by the noticeable decrease and increase of $\partial T_{c0}/\partial x(0, y)$ in the regions $0.2 < y < 0.75$ and $0.75 < y < 1$, respectively. Since energy is taken away from the region near the middle of the free surface, additional heat input is required to maintain $T(0, 0) = 1$. At $B = 10.0$, 1.0, 0.75 and 0.6 T, the values of $q_0 = 1.539$, 1.593, 1.627 and 1.669, respectively.

Figure 3(c) indicates that the position of maximum free-surface velocity $v_{p0}(0, y)$ shifts toward the wall as

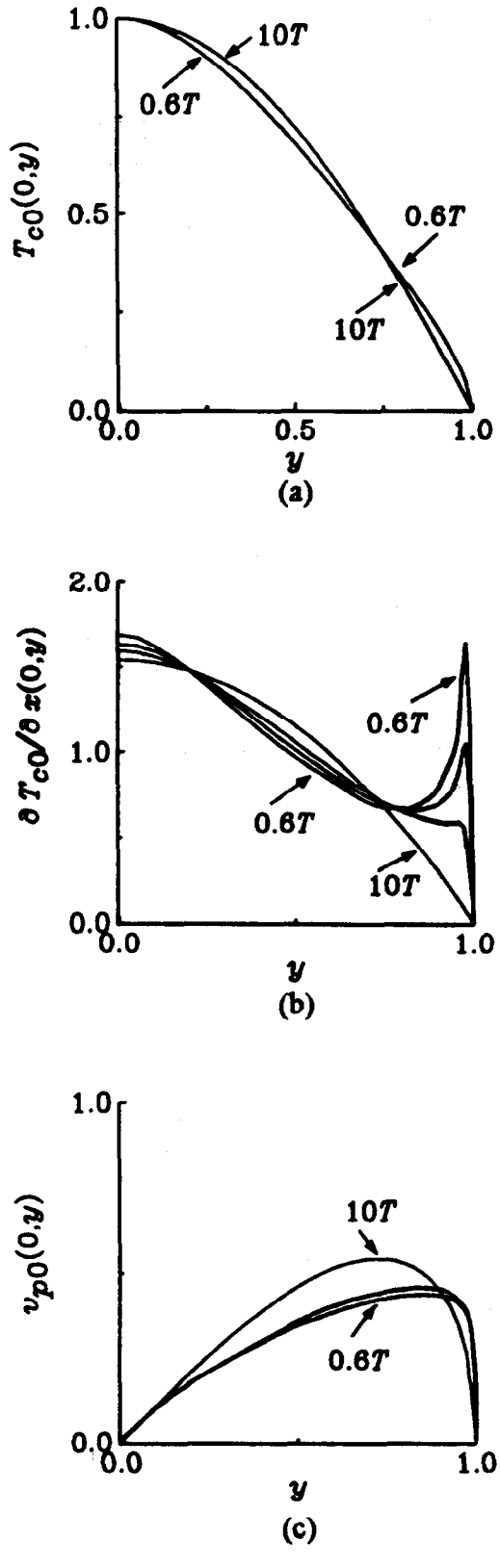

Fig. 3. (a) Surface temperature distribution $T_{c0}(0, y)$ for $B = 0.6$ and 10.0 T. (b) Heat flux entering the core $\partial T_{c0}(0, y)/\partial x$ for $B = 10.0$, 1.0, 0.75 and 0.6 T. (c) Free-surface velocity $v_{p0}(0, y)$ for $B = 10.0$, 0.75 and 0.6 T.

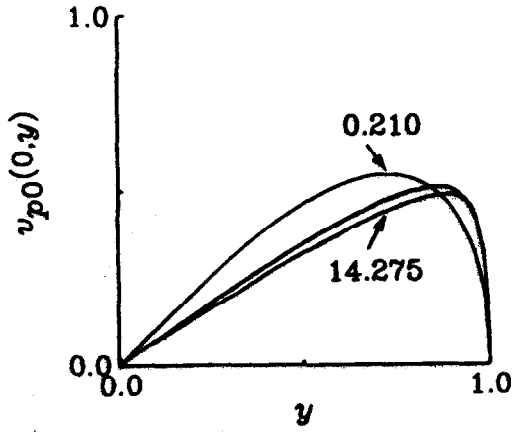

Fig. 4. Free-surface velocity $v_{p0}(0, y)$ for $\gamma = 0$ with $\alpha = 0.210$, 10.214 and 14.275.

B decreases. This shift, like the shift of ψ_{max}, can be attributed to the effects of inertia, but could also be due to an effect of heat convection that causes a larger surface-tension gradient near the wall region. At $B = 10.0$, 0.75 and 0.6 T, the maximum $v_{p0}(0, y)$ are 0.543, 0.462 and 0.440, and occur at $y = 0.725$, 0.860 and 0.900, respectively.

The temperature and flow solutions are inherently coupled in thermocapillary convection because the free-surface temperature gradient drives the liquid motion. Only by investigating the effects of inertia and convection independently can the nature of the heat transfer through the thermocapillary-driven, recirculating flow be fully described.

4.2. *Variable α with $\gamma = 0$*

The spectral code was run for the same values of α, but with $\gamma = 0$ so that there is no convective heat transfer. The heat flux entering the free surface is simply transferred by conduction through the parallel layer to the core region. No conduction occurs in the y-direction inside the parallel layer for large Ha. Although the surface-temperature distribution is not presented, $T_{c0}(0, y)$ is virtually identical to that shown in Fig. 3(a) for $B = 10$ T.

The values of $v_{p0}(0, y)$ for $\gamma = 0$ and $\alpha = 0.210$, 10.214 and 14.275 are shown in Fig. 4. As B decreases from 10.0 to 0.6 T, the inertial effects grow stronger, and shift the location of the maximum value of $v_{p0}(0, y)$ towards the wall at $y = 1$. At $\alpha = 0.210$, 10.214 and 14.275, $v_{p0}(0, y) = 0.544$, 0.506 and 0.490 at $y = 0.720$, 0.866 and 0.891, respectively. Whereas $v_{p0}(0, y)$ decreases as B decreases, the dimensional, maximum, free-surface velocity $10^3 v^*_{p0}(0, y) = 0.14$, 1.69 and 2.04 m s^{-1}, for $\alpha = 0.210$, 10.214 and 14.275, respectively, i.e. the dimensional velocity decreases by an order of magnitude with an order-of-magnitude increase of B.

Comparing the maximum $v_{p0}(0, y)$ with the results presented in Section 4.1 indicates that convective heat transfer has very little effect on the position of the maximum velocity. However, for $\alpha = 0.210$, 10.214

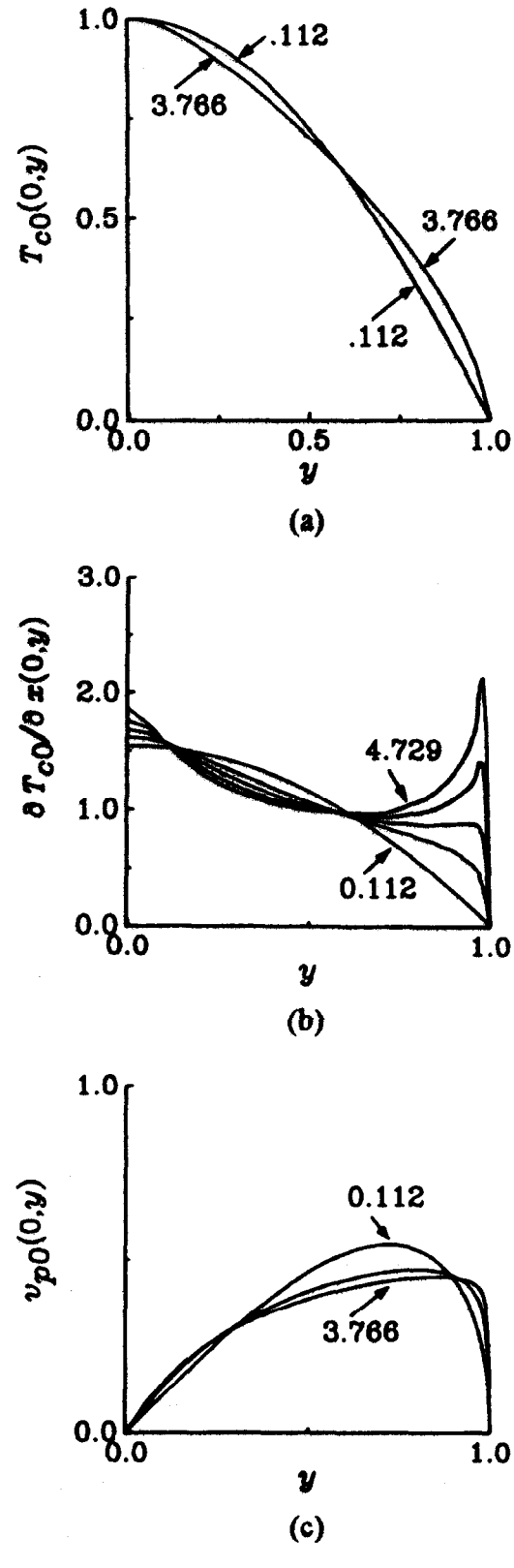

Fig. 5. (a) Surface temperature distribution $T_{c0}(0, y)$ for $\alpha = 0$ with $\gamma = 0.112$ and 3.766. (b) Heat flux entering the core $\partial T_{c0}(0, y)/\partial x$ for $\alpha = 0$ with $\gamma = 0.112$, 2.849, 3.766 and 4.729. (c) Free-surface velocity $v_{p0}(0, y)$ for $\alpha = 0$ with $\gamma = 0.112$, 2.849 and 3.766.

and 14.275, the maximum $v_{p0}^{*}(0, y)$ is decreased by the influence of convective heat transfer by 0.2, 9.5 and 11.4%, respectively, because the convection alters the free-surface temperature distribution, which in turn affects the thermocapillary force that drives the flow.

4.3. *Variable γ with $\alpha = 0$*

Figure 5(a) shows $T_{c0}(0, y)$ for $\gamma = 0.112$ and 3.766 which correspond to those values of γ for $B = 10$ and 0.6 T, respectively, but with $\alpha = 0$. A comparison of Fig. 3(a) with Fig. 5(a) indicates that the elimination of inertial effects produces a lower temperature near the center of the free surface, and a higher temperature near the wall. Figure 5(c) shows $v_{p0}(0, y)$ for $\gamma = 0.112$, 2.849 and 3.766, and $\alpha = 0$. A comparison of these velocity profiles with those shown in Fig. 3(c) at the corresponding values of $B = 10.0$, 0.75 and 0.6 T, indicates that the absence of inertial effects allows the fluid to accelerate to higher values of $v_{p0}(0, y)$ near the middle of the free surface, so that there is more convective heat transfer for a given γ with $\alpha = 0$ than with the actual values of α. The maximum $v_{p0}(0, y) = 0.543$, 0.471 and 0.451 occurred at $y = 0.707$, 0.809 and 0.839 for $\gamma = 0.112$, 2.849 and 3.766, respectively, corresponding to an increase in $v_{p0}(0, y)$ by 0.0, 2.0 and 2.5% due to the absence of inertial effects. Similarly, the absence of inertial effects caused the maximum y location of $v_{p0}(0, y)$ to decrease by 2.5, 5.9 and 6.8%, respectively. At $\gamma = 0.112$, 2.849 and 3.766, the values of $q_0 = 1.750$, 1.674 and 1.539, which correspond to an increase in q_0 by 0, 2.9 and 4.9%, respectively, also due to the absence of inertial effects.

The heat flux into the core $\partial T_{c0}/\partial x(0, y)$ is shown in Fig. 5(b) for $\gamma = 0.112$, 1.988, 2.849, 3.766 and 4.729, which correspond to values of $B = 10$, 1.0, 0.75, 0.6 and 0.5 T, with $\alpha = 0$. Also included is the $B = 0.5$ T case with $\alpha = 0$; however, no comparison can be made with Fig. 3(b) because no solution could be found with $\alpha = 18.765$ and $\gamma = 4.729$. Comparing results for those values of γ which correspond to $B = 0.75$ and 0.6 T shows that $\partial T_{c0}/\partial x(0, y)$ is lower for $0 < y < 0.5$, and much larger for $0.5 < y < 0.9$. This decrease and increase in $\partial T_{c0}/\partial x(0, y)$ is due to the higher velocities near the middle of the free surface convecting heat from $0 < y < 0.5$ to $0.5 < y < 0.9$. Yet, in the absence of inertia, the free-surface velocities are nearer to the wall, so that more heat is convected in the region $0.9 < y < 1.0$ when inertia is included, and causes the sharp rise in the core heat flux in that region.

5. CONCLUSION

The model presented here represents the floating-zone process that is used to grow high-perfection, single-crystal semiconductors. Since thermocapillary convection is a cause of defects in the floating-zone process, an understanding of the heat transfer and fluid motion in the process is needed in order to grow defect-free crystals. In the presence of a strong axial DC magnetic field, the thermocapillary convection is confined to a thin boundary layer adjacent to the free surface, leaving a quiescent inner core region. The heat flux entering the free surface is redistributed in the thin boundary layer when Pe is $O(Ha^{1/4})$, where Ha is the large Hartmann number, and is proportional to the applied magnetic flux density B. The asymptotic analysis also revealed that the strong inertial effects, which led to the detrimental unsteady thermocapillary convection in floating-zone process, were eliminated at large magnetic flux densities, as was the convective heat transfer. Furthermore, an order-of-magnitude decrease in the volumetric flow rate was observed with an order-of-magnitude increase in the magnetic flux density.

Acknowledgments—This research was supported by the National Science Foundation under Grant CTS-94-19484, and by the National Aeronautics and Space Administration under Cooperative Research Agreement NCC8-90.

REFERENCES

1. Cröll, A., Dold, P. and Benz, K. W., Segregation in Si floating-zone crystals grown under microgravity and in a magnetic field. *Journal of Crystal Growth*, 1994, **137**, 95–101.
2. Series, R. W. and Hurle, D. T. J., The use of magnetic fields in semiconductor crystal growth. *Journal of Crystal Growth*, 1991, **113**, 305–328.
3. Robertson, G. D. and O'Connor, D., Magnetic field effects on float-zone Si crystal growth III. Strong axial fields. *Journal of Crystal Growth*, 1986, **76**, 111–122.
4. Müller, G. and Rupp, R., The role of Marangoni convection in the growth of GaAs crystals by the floating zone technique under microgravity. *Crystal Properties and Preparation*, 1991, **35**, 138–154.
5. Rupp, R., Auerochs, S., Müller, G., Weyrich, C. and Leibenzeder, S., Growth of GaAs single crystals by the floating zone technique under microgravity. *Advanced Space Research*, 1991, **11**, 297–304.
6. Morthland, T. E. and Walker, J. S., Thermocapillary convection during floating-zone silicon growth with a uniform or non-uniform magnetic field. *Journal of Crystal Growth*, 1996, **158**, 471–479.
7. Hjellming, L. N. and Walker, J. S., Melt motion in a Czochralski crystal puller with an axial magnetic field: motion due to buoyancy and thermocapillarity. *Journal of Fluid Mechanics*, 1987, **182**, 335–368.
8. Khine, Y. Y. and Walker, J. S., Thermocapillary convection in a cylinder with a strong nonuniform axisymmetric magnetic field. *Journal of Fluid Mechanics*, 1994, **276**, 369–388.
9. Langlois, W. E. and Lee, K. J., Czochralski crystal growth with an axial magnetic field: effects of Joulean heating. *Journal of Crystal Growth*, 1983, **62**, 481–486.
10. Hunt, J. C. R. and Leibovich, S., Magnetohydrodynamic flow in channels of variable cross-section with strong transverse magnetic field. *Journal of Fluid Mechanics*, 1967, **28**, 241–260.
11. Walker, J. S., Ludford, G. S. S. and Hunt, J. C. R., Three-dimensional MHD duct flows with strong transverse magnetic fields. Part 3. Variable-area rectangular ducts with insulating walls. *Journal of Fluid Mechanics*, 1972, **56**, 121–141.
12. Morthland, T. E. and Walker, J. S., Inertial effects in magnetically stabilized thermocapillary convections during floating-zone semiconductor crystal growth in space. *Journal of Crystal Growth*, 1997.